

Ultrabroadband Super-Planckian Radiative Heat Transfer with Profile-Patterned Hyperbolic Metamaterial

Jin Dai,¹ Fei Ding,² Sergey I. Bozhevolnyi,² and Min Yan¹

¹*Department of Materials and Nano Physics,
School of Information and Communication Technology,
KTH-Royal Institute of Technology,
Electrum 229, 16440 Kista, Sweden**

²*Centre for Nano Optics, University of Southern Denmark,
Campusvej 55, DK-5230 Odense, Denmark*

(Dated: June 17, 2019)

Abstract

We demonstrate the possibility of ultrabroadband super-Planckian radiative heat transfer between two metal plates patterned with tapered hyperbolic metamaterial arrays. It is shown that, by employing profile-patterned hyperbolic media, one can design photonic bands to populate a desired thermal radiation window, with a spectral density of modes much higher than what can be achieved with unstructured media. For nanometer-sized gaps between two plates, the modes occupy states both inside and outside the light cone, giving rise to ultrabroadband super-Planckian radiative heat transfer. Our study reveals that structured hyperbolic metamaterial offers unprecedented potential in achieving a controllable super-Planckian radiative heat transfer.

PACS numbers: 44.40.+a, 73.20.Mf

Hyperbolic metamaterials (HMMs) are highly anisotropic artificial materials with both positive and negative permittivity tensor components. The name comes from their distinct hyperbolic photonic dispersion curves when examined in bulk. Over the past decade, HMMs have been realized by a series of configurations, including metal-dielectric multilayer structures, nanowire arrays embedding in a dielectric matrix, etc [1]. Thanks to their unique dispersion property, HMMs can manipulate electromagnetic field in many unconventional ways and have inspired a range of exotic applications. For example, hyperlenses, which can overcome the diffraction limit, have been demonstrated utilizing a curved multilayer HMM for super-resolution imaging [2, 3]. HMMs have also been used to engineer thermal emitters emission properties, including directionality, coherence, and polarization [4]. Very recently, enhanced radiative heat transfer (RHT) in the near-field regime using HMMs has come in the fore. These near-field investigations are mainly based on two types of structures: (i) HMMs formed by a multi-bilayer stack made of phonon-polaritonic metal, such as SiC or heavily doped Si, and dielectric [5–7]; (ii) nanowire arrays consisting of phonon-polaritonic metals embedded in a dielectric matrix [8, 9]. In these studies, no profile-patterning of the hyperbolic media was introduced, and the RHT phenomena were therefore determined by the bulk material properties of hyperbolic media. In addition, in the studies [8, 9], each nanowire array was unexceptionally treated as a semi-infinite homogenized layer of effective anisotropic material. The effective medium theory (EMT) cannot always precisely predict RHT between two closely spaced nanowire arrays or two multilayer HMMs, even for a gap size larger than the periodicity in the metamaterial [10, 11].

In this Letter, we consider the RHT between metamaterial plates consisting of arrays of tapered multilayered metal-dielectric stacks. Individual arrays of these stacks were previously found to exhibit broadband absorption of far-field radiation [12]. Near-field properties with implications to RHT were insofar left unexplored. It turns out the profile-patterned hyperbolic media exhibit ultrabroadband spectra of electromagnetic modes both inside and outside the light cone, with an exceptionally high packing density in infrared frequencies relevant to most RHT situations. Moreover, the electromagnetic properties of the structured hyperbolic media can be adaptively tuned through geometrical modification towards different applications. Using a rigorous full-wave scattering-matrix method, we calculate the RHT flux between two patterned metamaterial plates and show that, for gap sizes smaller than the thermal wavelength, the flux can indeed exceed that of the blackbody limit, not

only at specific (isolated) frequencies but practically over the whole spectrum. We utilize a complex eigenvalue mode solver to reveal the modal properties of the double-plate structure and identify that surface plasmon polaritons (SPPs), gap surface plasmons (GSPs), and hybrid waveguide modes play critical roles in enhancing near-field RHT.

The representative structure under investigation is depicted in Fig. 1. It consists of two identical 1D periodic tapered HMMs arrays on a metal substrate separated by a vacuum gap g . Each tapered HMMs cavity is formed by 20 dielectric-metal pairs. The relative permittivity of metal (Au) and dielectric (Si) are $\epsilon_{\text{Au}}(\omega) = 1 - \frac{\omega_p^2}{\omega(\omega+i\gamma)}$, in which $\omega_p = 9$ eV, and $\gamma = 35$ meV, and $\epsilon_{\text{Si}} = 11.7$, respectively. The thicknesses of dielectric and metal are fixed at $t_d = 95$ nm and $t_m = 20$ nm. The cross-section of a single stack resembles a trapezoid with short base of $w_t = 400$ nm, long base of $w_b = 1900$ nm, and height of $h = (t_d + t_m) \times 20 = 2.3$ μm . Each individual layer has vertical sides. The period of the HMMs arrays is fixed at $a = 2000$ nm. Such structure can be fabricated with focused ion beam milling of deposited metal-dielectric multilayers [13], or with shadow deposition of dielectric and metal layers [14, 15]. The multilayered metal-dielectric material, when unpatterned, has an *indefinite* effective permittivity tensor, where x and y components are negative whilst z component is positive.

The radiative heat flux between two 1D periodic arrays can be expressed by

$$q(T_1, T_2) = \frac{1}{2\pi} \int_0^\infty [\Theta(\omega, T_1) - \Theta(\omega, T_2)] \Phi(\omega) d\omega, \quad (1)$$

in which $\Theta(\omega, T) = \hbar\omega / \exp[(\hbar\omega/k_B T) - 1]$ is the mean energy of Planck oscillators of temperature T with angular frequency ω . $\Phi(\omega)$ is the integrated transmission factor given by

$$\Phi(\omega) = \frac{1}{4\pi^2} \sum_{j=\text{s,p}} \int_{-\infty}^{+\infty} \int_{-\frac{\pi}{a}}^{+\frac{\pi}{a}} \mathcal{T}_j(\omega, k_x, k_y) dk_x dk_y. \quad (2)$$

$\mathcal{T}_j(\omega, k_x, k_y)$ is the transmission factor that describes the probability of a thermally excited photon of either s-polarization or p-polarization, with surface-parallel wavevectors (k_x, k_y) at angular frequency ω transferring from the one plate to the other. To calculate transmission factor, we employ a scattering approach and the details of this method can be found in Refs. 16 and 17.

Figure 2 plots the transmission factor $\mathcal{T}_j(\omega, k_x, 0)$ between plates with such two tapered HMM arrays for surface-parallel wavevector along x direction. The calculation is repeated

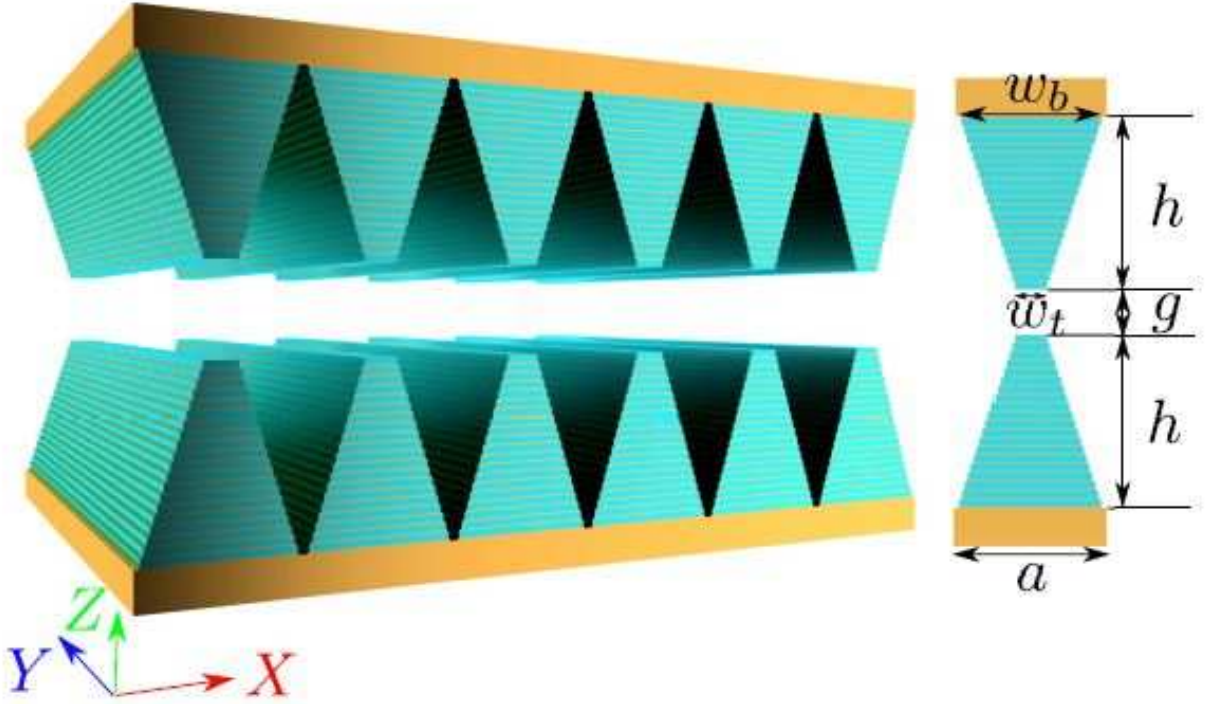


FIG. 1. (Color online). Schematic of the proposed tapered hyperbolic metamaterial gratings. The temperatures of the bottom- (hot) and top- (cold) plate are T_1 and T_2 respectively. The cyan layers denote dielectric and the golden layer denote gold.

for four gap sizes: 5000, 1000, 500, and 50 nm. For a larger gap size $g = 5000$ nm, the contributions are mainly from the propagating modes above the light line. The brighter part, which has a maximum value close to two, are due to degenerate s- and p-polarized modes. The s-polarized contribution to RHT comes from guided modes mostly inside the vacuum gap, as characterized by a low-frequency cutoff in the transmission-factor map. The hyperbolic medium behaves like a metal for s-polarized light as dictated by the materials negative permittivity along y direction (electric field direction of s-polarization). The contribution from s-polarization is not present for smaller gap sizes, because the cutoff frequency for the s-polarized mode gets higher for smaller gap sizes, a characteristics analogous to guided s modes in a metal-slot waveguide. The contribution to RHT from p-polarized light exists more extensively, both above (propagating modes) and below (surface modes) light line. The two low-frequency surface-mode bands become more separated as gap size decreases. The two bands, as will be shown in Fig. 3, correspond to a bonding and anti-bonding mode pair resulted from splitting of SPPs supported by individual gold-HMM interfaces. For p-

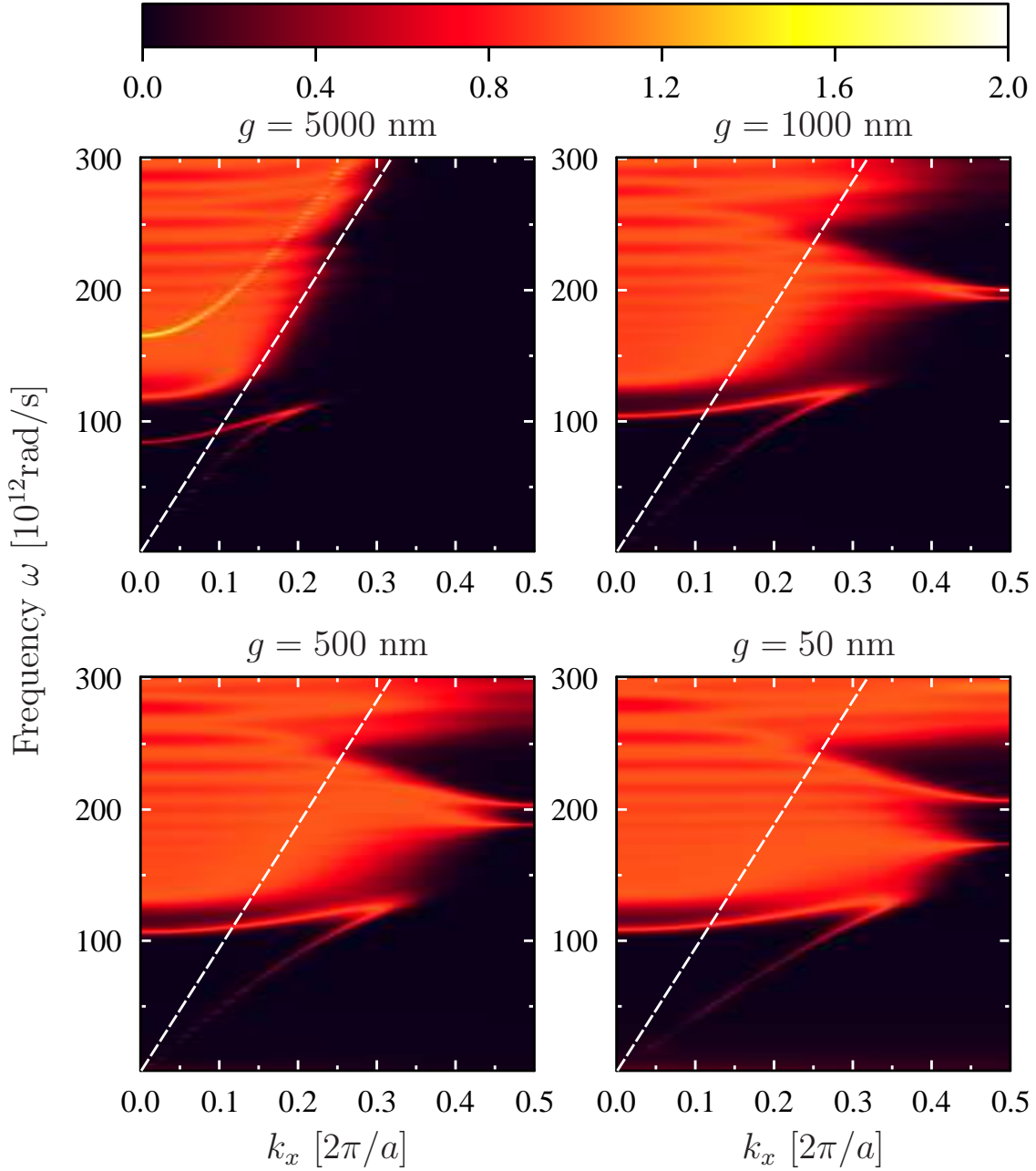


FIG. 2. (Color online). Transmission factor $\mathcal{T}_j(\omega, k_x, 0)$ between two tapered hyperbolic meta-material gratings at different gap sizes $g=5000$ nm, $g=1000$ nm, $g=500$ nm, and $g=50$ nm. The dashed white line indicates the light line in vacuum.

polarization, besides the two low-frequency bands, the structure presents an ultrabroadband transmission factors. High transmission factor extends even to k_x values at the Brillouin zone edge, i.e. $k_x = \frac{\pi}{a}$, for smaller gaps. From the plots in Fig. 2, it is apparent that the

tapered HMM-based plates not only can achieve far-field RHT close to blackbody limit, but also, when their separation is small, can achieve super-Planckian RHT by making use of most near-field states.

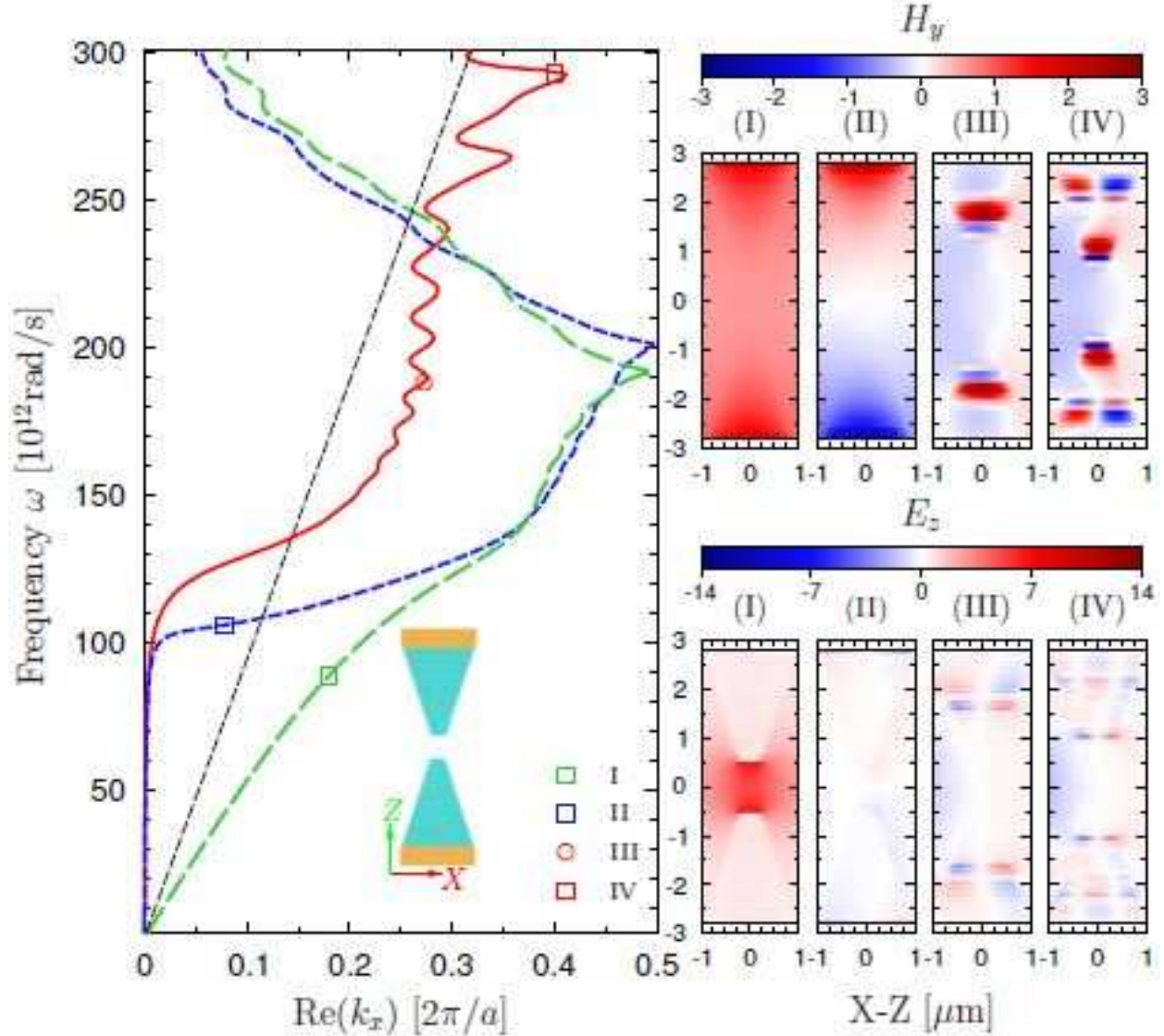


FIG. 3. (Color online). The dispersion relation between two tapered hyperbolic metamaterial arrays with $g = 1000$ nm along x direction. And the field distributions of the marked points on the dispersion curves.

To unveil the underlying physical mechanism for p-polarized transmission factors, which play a major role in the RHT for the considered surface-parallel wavevectors, we solve the dispersion relation of the p-polarized modes using a finite-element-based *complex wavenum-*

ber eigensolver [18, 19]. The real part of $k_x(\omega)$ for p-polarized modes and the representative H_y and E_z fields in x-z plane are shown in Fig. 3. Modes I-II manifest a bonding and anti-bonding SPP modes pair which is similar to that supported by metal-insulator-metal (MIM) plates structure. Since the modes carry their electric field components oriented majorly along z direction, the tapered HMM stack can be effectively treated as a dielectric material. The anti-bonding mode exhibits a lower cutoff frequency, while the bonding mode has not. Modes III-IV show typical gap-plasmon-like modes featuring enhanced magnetic fields [20–22]. Each tapered HMM stack can be treated as a series of gap-plasmon resonators with varying widths. The resonant frequency of each resonator depends on its width, which dictates such a tapered HMM stack has an ultrabroadband resonance coupled to propagating modes (i.e. states above light line). Mode IV shows a second-order gap plasmon excited at the base of the HMM stack where the resonator is wider; simultaneously a first-order gap-plasmon resonance is excited at a narrower part of the stack. In Supplemental Material, we present similar transmission-factor map as well as modal dispersion curves for a rectangular HMM arrays. In that case, since the gap-plasmon resonators in a single HMM stack have the same width, the gap-plasmon bands are much less in number and occupy a narrower frequency range. The appearance of multiple bands is a result of multimode resonances owing to a finite height of the HMM stacks. Note also that these gap-plasmon modes are also forming bonding and anti-bonding pairs due to adjacency of the two plates, which is clearer for the rectangular HMM array case (see Supplemental Materials).

A full characterization of RHT between two plates requires a calculation of transmission coefficients for all surface-parallel wavevectors over a frequency range relevant to temperature setting. Besides transmission-coefficient maps shown in Fig. 2, we computed transmission coefficient for all possibility surface parallel wavevectors. We selectively plot the transmission factor $\mathcal{T}_j(\omega, k_x, k_y)$ at $\omega = 172.73$ [10^{12} rad/s] in Fig. 4 for different gap sizes. For larger gap sizes, the contributions mainly come from both s- and p-polarized propagating modes (inside light cone). It is interesting to notice that, at the gap size of $g = 5000$ nm, the distributions of transmission factors for s- and p-polarizations are almost complementary to each other; addition of them would lead to nearly unitary transmission factor filling the whole light cone. As the gap size decreases, the contribution from modes outside the light cone becomes dominant, suggesting more and more near-field interactions. At $g = 1000$ nm, the heat flux at this frequency is already beyond the far-field blackbody limit [see Fig. 5(a-b)]. Both

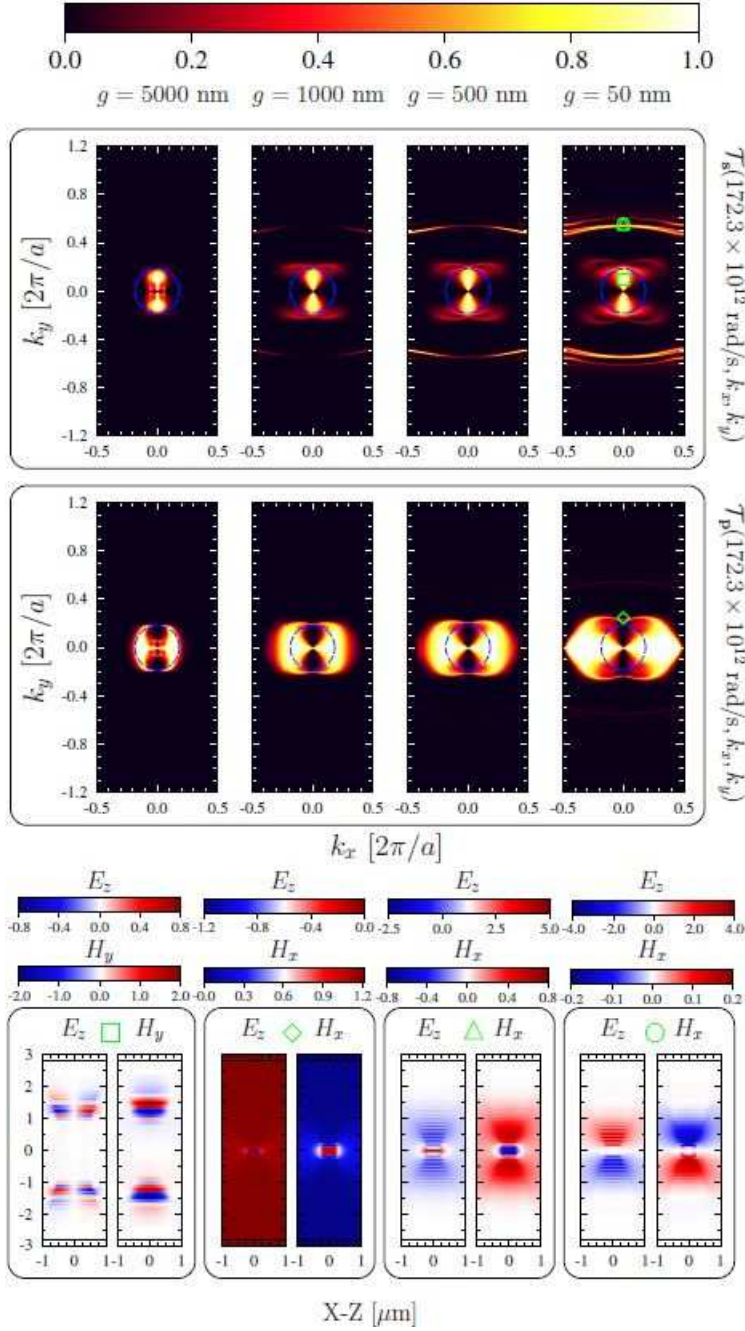


FIG. 4. (Color online). The transmission factor $\mathcal{T}_j(\omega, k_x, k_y)$ of s- (top) and p- (middle) polarizations for the structure depicted in Fig 1 with different gap sizes of $g = 5000$ nm, $g = 1000$ nm, $g = 500$ nm. Angular frequency is fixed at $\omega = 172.73$ [10^{12} rad/s]. The blue-dashed lines denote the light cones in vacuum. The mode profiles corresponding to the marks on the transmission-factor maps (for $g = 50$ nm configuration) are plotted (bottom).

s- and p-polarizations contribute to RHT over a broad (k_x, k_y) combinations. To better

understand these RHT channels, we plot four representative mode fields, as marked on the transmission-factor maps in Fig. 4, all corresponding to the $g = 50$ nm configuration. Since mode patterns for $(k_x \neq 0, k_y = 0)$ were presented in Fig. 3, here we examine modes with $(k_x = 0, k_y \neq 0)$. These modes are nothing but guided modes by the HMM array. It is easy to imagine that each tapered HMM stack, being structurally invariant in y direction, functions like an optical waveguide [23]; a single HMM grating is simply a waveguide array; two gratings form a super-waveguide array. Due to very high contrast in permittivity values, the guided modes are hybrid in polarization, which means they can be excited by either s- or p-polarized light. The mode inside the light cone, as marked by the green square, manifests a gap-plasmon mode, propagating along y while radiating out to free space. Again for s-polarization, there exists a series of modes outside light cone; the first two are marked by the green triangle and circle: These two modes are due to bonding and anti-bonding couplings between the fundamental modes supported by each HMM grating. It is worth noting that, unlike all dielectric waveguides, these hybrid modes supported by HMM waveguide exhibit a reverse ordering, i.e. higher order with a larger k_y , due to the indefinite permittivity tensor [14, 23]. The mode marked by the green diamond indicates a gap-plasmon-like mode mainly confined inside the air gap between the two HMM arrays, which does not exist in an individual HMM array.

Finally, in Fig. 5(a) we plot the integrated transmission factor spectra $\Phi(\omega)$ between the two HMM arrays at different gap sizes. We also superimpose the spectrum for two blackbodies. At lower frequencies the HMM array shows a higher transmission factor than the blackbody. This is mainly contributed by the coupling between waveguide modes of the tapered HMM waveguide and the gap-plasmon-like modes inside the air gap. The coupling of gap plasmon modes between two HMM arrays starts playing an important role for angular frequency above around 120×10^{12} rad/ss (refer to Fig. 2). As the gap size decreases down to 50 nm, the transmission factors between two HMM arrays get beyond that between two blackbodies almost over all the spectra range we studied, which enables us to achieve ultrabroadband super-Planckian RHT. We demonstrate super-Planckian radiation by comparing the spectral heat flux between two HMM arrays with temperature $T_1 = 301$ K, $T_2 = 300$ K to that between two blackbodies with the same temperatures configuration in Fig. 5(b). At the very near field with $g = 50$ nm, HMM array performs much better than blackbodies, range from 4.4 to 1236 times of that between two blackbodies across the whole

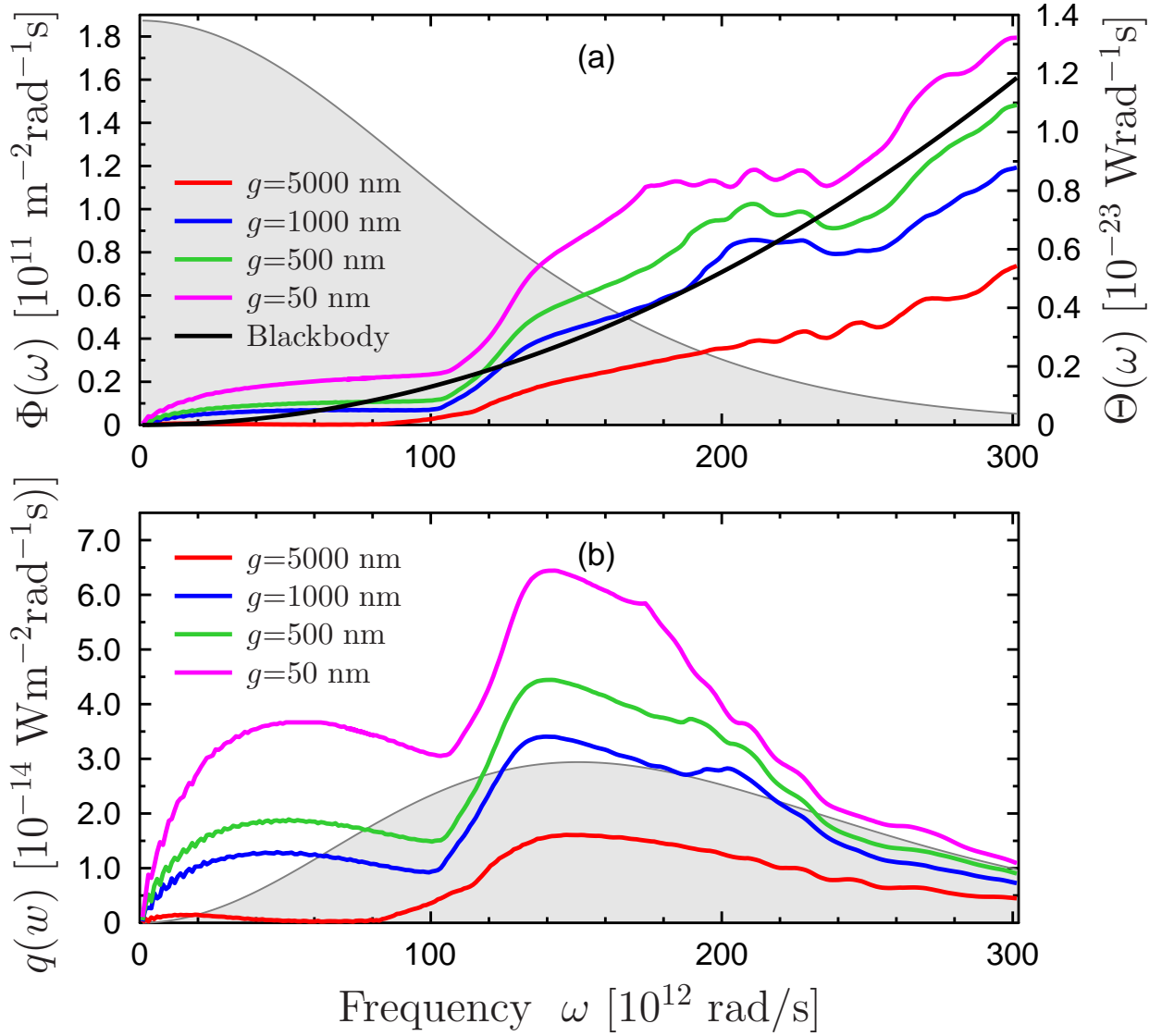


FIG. 5. (Color online). (a) Integrated transmission factor spectra $\Phi(\omega)$ for the structure depicted in Fig. 1 with gap size of $g = 5000$ nm, $g = 1000$ nm, $g = 500$ nm, and $g = 50$ nm and that between two blackbodies. (b) Spectral heat flux $q(\omega)$ for the same configuration as shown in (a) for $T_1 = 301$ K and $T_2 = 300$ K. The gray lines with shading in (a) and (b) indicate Planck's oscillator term $\Theta(\omega, 301\text{ K}) - \Theta(\omega, 300\text{ K})$

and spectral heat flux between two blackbodies respectively.

spectra range we studies. We predict that the performance can be even improved by using 2D periodic HMM pyramids arrays which support GSP resonance for both s- and p-polarized

photon with almost all surface-parallel wavevector directions [13].

In conclusion, we have demonstrated an ultrabroadband super-Planckian RHT between two closely spaced tapered HMM arrays using an exact scattering approach instead of EMT. We have explicitly explained the role of GSP resonances, SPP resonances and hybrid waveguide modes by analyzing field distributions of the corresponding modes which give the major contributions in transmission-factor maps. We reveal that, unlike the modes supported by homogeneous multilayered HMM [5] or nanowire arrays [8, 9], which are strongly dependent on filling ratio between metals and dielectrics and their material properties, these modes are also geometry dependent, which gives another degree of freedom to further engineer the spectral properties of near-field RHT. Our study opens up a new route for achieving controllable super-Planckian RHT with structured hyperbolic metamaterials.

J. D. and M. Y. acknowledge the support by the Swedish Research Council (Vetenskapsrådet or VR) via Project No. 621-2011-4526, and VR's Linnaeus center in Advanced Optics and Photonics (ADOPT). F. D. and S. I. B. acknowledge financial support from the Danish Council for Independent Research (the FTP project PlasTPV, Contract No. 1335-00104). The simulations were performed on resources provided by the Swedish National Infrastructure for Computing (SNIC) at PDC Centre for High Performance Computing (PDC-HPC).

* e-mail: jind@kth.se

- [1] A. Poddubny, I. Iorsh, P. Belov, and Y. Kivshar, *Nat. Photon.* **7**, 948 (2013).
- [2] Z. Liu, H. Lee, Y. Xiong, C. Sun, and X. Zhang, *Science* **315**, 1686 (2007).
- [3] J. Rho, Z. Ye, Y. Xiong, X. Yin, Z. Liu, H. Choi, G. Bartal, and X. Zhang, *Nat. Commun.* **1**, 143 (2010).
- [4] S. S. Kruk, Z. J. Wong, E. Pshenay-Severin, K. O'Brien, D. N. Neshev, Y. S. Kivshar, and X. Zhang, *Nat. Commun.* **7** (2016).
- [5] S.-A. Biehs, M. Tschikin, R. Messina, and P. Ben-Abdallah, *Appl. Phys. Lett.* **102**, 131106 (2013).
- [6] Y. Guo and Z. Jacob, *Opt. Express* **21**, 15014 (2013).
- [7] Y. Guo, C. L. Cortes, S. Molesky, and Z. Jacob, *Appl. Phys. Lett.* **101**, 131106 (2012).

- [8] S.-A. Biehs, M. Tschikin, and P. Ben-Abdallah, *Phys. Rev. Lett.* **109**, 104301 (2012).
- [9] X. Liu, R. Z. Zhang, and Z. Zhang, *ACS Photonics* **1**, 785 (2014).
- [10] M. Tschikin, S.-A. Biehs, R. Messina, and P. Ben-Abdallah, *J. Opt.* **15**, 105101 (2013).
- [11] M. S. Mirmoosa, F. Rütting, I. S. Nefedov, and C. R. Simovski, *J. Appl. Phys.* **115**, 234905 (2014).
- [12] Y. Cui, K. H. Fung, J. Xu, H. Ma, Y. Jin, S. He, and N. X. Fang, *Nano Letters* **12**, 1443 (2012).
- [13] F. Ding, Y. Jin, B. Li, H. Cheng, L. Mo, and S. He, *Laser Photon. Rev.* **8**, 946 (2014).
- [14] X. Yang, J. Yao, J. Rho, X. Yin, and X. Zhang, *Nat. Photon.* **6**, 450 (2012).
- [15] J. Zhou, A. F. Kaplan, L. Chen, and L. J. Guo, *ACS Photonics* **1**, 618 (2014).
- [16] R. Guérout, J. Lussange, H. B. Chan, A. Lambrecht, and S. Reynaud, *Phys. Rev. A* **87**, 052514 (2013).
- [17] J. Dai, S. A. Dyakov, and M. Yan, *Phys. Rev. B* **93**, 155403 (2016).
- [18] G. Parisi, P. Zilio, and F. Romanato, *Opt. Express* **20**, 16690 (2012).
- [19] C. Fietz, Y. Urzhumov, and G. Shvets, *Opt. Express* **19**, 19027 (2011).
- [20] S. I. Bozhevolnyi and T. Søndergaard, *Opt. Express* **15**, 10869 (2007).
- [21] J. Jung, T. Søndergaard, and S. I. Bozhevolnyi, *Phys. Rev. B* **79**, 035401 (2009).
- [22] J. Hao, J. Wang, X. Liu, W. J. Padilla, L. Zhou, and M. Qiu, *Appl. Phys. Lett.* **96**, 251104 (2010).
- [23] M. Yan, L. Thylén, and M. Qiu, *Opt. Express* **19**, 3818 (2011).

Ultrabroadband Super-Planckian Radiative Heat Transfer with Profile-Patterned Metamaterial-Supplemental material

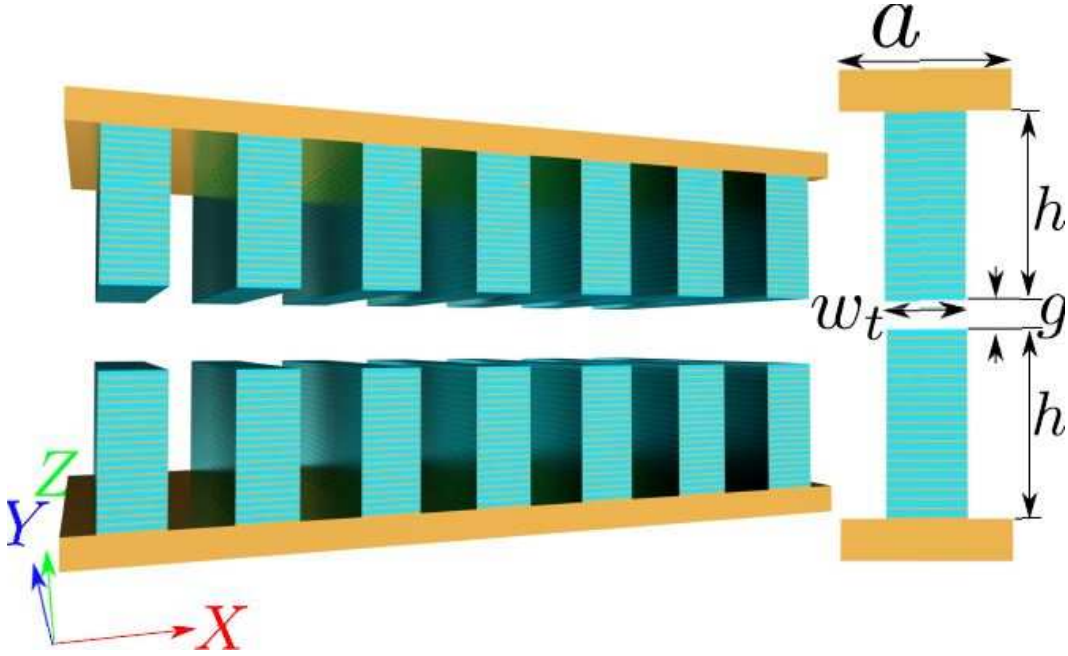


FIG. 6. (Color online). Schematic of a double plates with rectangular hyperbolic metamaterial gratings. The cyan layers denote dielectric and the golden layer denote gold.

The periodic tapered hyperbolic metamaterial (HMM) based double-plated system studied in the main text supports numerous and complicated electromagnetic resonances. Here we use a simplified structure to facilitate easier understanding of the enhanced radiative heat transfer (RHT) phenomenon. Namely, instead of using a tapered HMM stack, here we use a rectangular one. The schematic of a double plate system with HMM gratings is depicted in Fig. 6. Each plate consists of a periodic HMM stack. Each stack has 20 pairs of dielectric-metal bilayers with a period of $a = 2000$ nm on a gold substrate. The thicknesses of dielectric and metal are fixed at $t_d = 95$ nm and $t_m = 20$ nm. The width of the rectangular HMM stacks is $w_t = 1000$ nm. Figure 7 shows the transmission factor $\mathcal{T}_j(\omega, k_x, k_y = 0)$ between two such rectangular HMM arrays as a function of angular frequency and surface-parallel wavevector along x direction. In the same plot, we also superimpose the calculated real k_x v.s. ω dispersion curve based on eigen-mode analysis. Such a comparison helps us to identify the nature of the modes contributing to the RHT process. To gain further knowledge of these modes, we plot the relations corresponding to

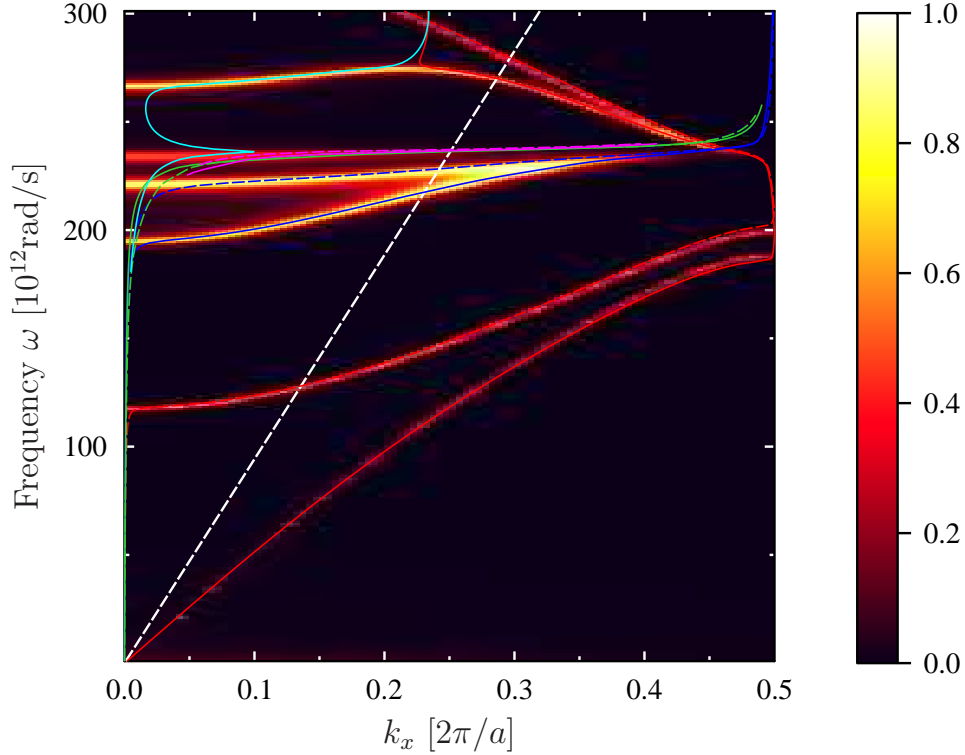


FIG. 7. (Color online). Transmission factor $\mathcal{T}_j(\omega, k_x, 0)$ between two rectangular hyperbolic meta-material arrays with width of $w_t = w_b = 1000$ nm at gap sizes $g=1000$ nm. The dashed white lines indicate the light lines in vacuum. The real k_x vs ω from Fig. 8 are plotted on top of the transmission factor map.

frequency v.s. both real and imaginary parts of the wavevectors of these modes, as well as their representative electromagnetic field distributions in Fig. 8. For field distributions, the color maps present the y component of magnetic field and the arrow maps present the electric field in x - z plane. Field distributions at point (I) and (II) manifest the red bands are bonding and anti-bonding surface plasmon polariton modes supported between two gold substrate filled by a two rectangular HMM gratings (with an air gap in between). Since for this pair of modes, light is majorly polarized in z direction, the HMM grating can be treated as a dielectric grating with relative permittivity $\epsilon = \epsilon_z = \frac{\epsilon_{\text{Au}}\epsilon_{\text{Si}}}{(1-f)\epsilon_{\text{Au}} + f\epsilon_{\text{Si}}}$. Here f is the filling ratio of gold. Field distributions at point (III)-(VIII) show the higher-order modes. Field patterns show these modes are less coupled between periods, suggesting their less dispersive

bands or more resonator-like resonance nature. The resonance frequencies of such modes are heavily determined by the width of the rectangular HMM. On top of that, they are also determined the round-trip phase condition as they make a vertical (along z) round trip in a HMM stack. In the extremely high-order case, the mode would be approach to the so-called magnetic-dipole-like or gap-plasmon resonances supported by metal-insulator-metal structure. Since the separation between the two rectangular HMM plates are small, strong coupling between them creates bonding and anti-bonding mode pairs. The higher z order modes have larger imaginary parts, which lead to weaker contributions to RHT. By having a tapered HMM array, which has a gradually changing cavity width, one can obtain an ultrabroadband resonances, resulting in super-Planckian radiative energy transfer.

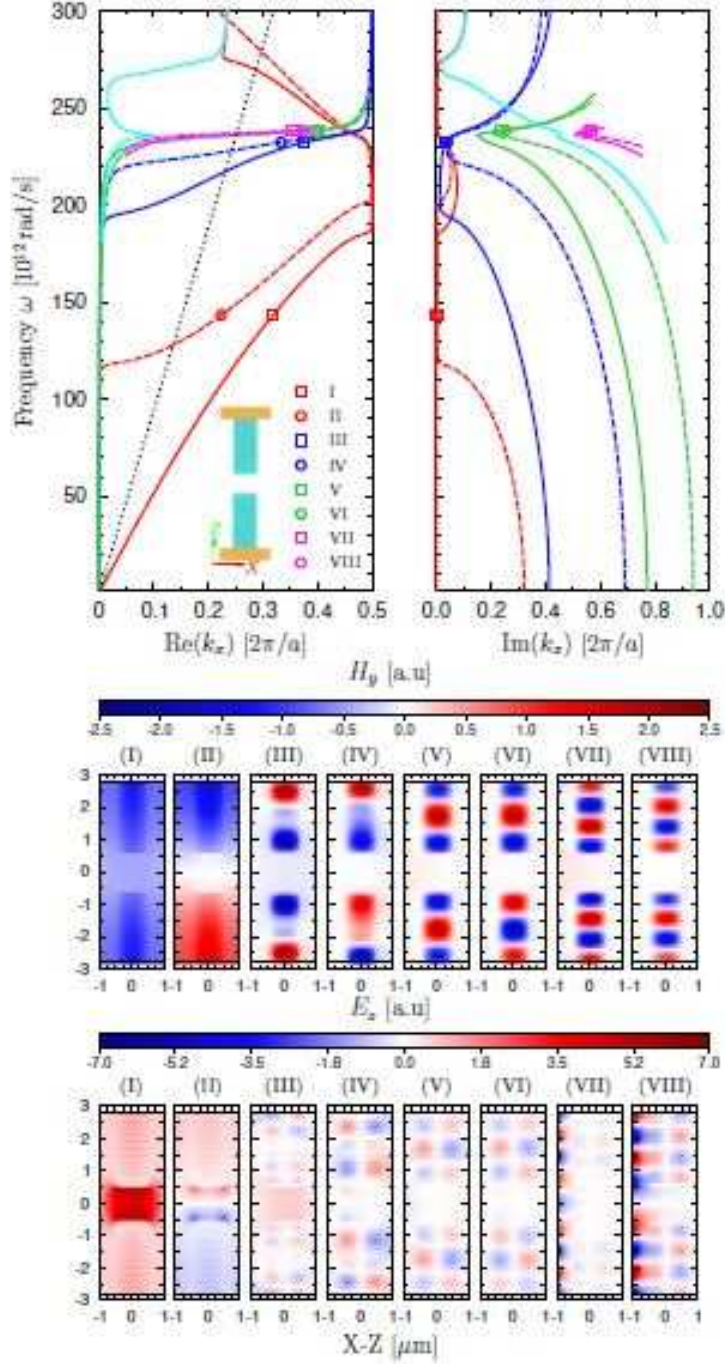


FIG. 8. (Color online). The dispersion relation between two rectangular hyperbolic metamaterial arrays with width of $w_t = w_b = 1000$ nm and gap of $g = 1000$ nm along x direction . And the field distributions of the marked points on the dispersion curves. The color maps present the y component of the magnetic field and the arrow maps presents the electric field in x - z plane.